2-10-2009

Size-dependent magnetic properties of high oxygen content YMn2O5±δ multiferroic nanoparticles

C. Ma
Iowa State University

J.-Q. Yan
Iowa State University

Kevin W. Dennis
Iowa State University, dennis@ameslab.gov

R. William McCallum
Iowa State University, mccallum@ameslab.gov

Xiaoli Tan
Iowa State University, xtan@iastate.edu

Size-dependent magnetic properties of high oxygen content $YMn_2O_{5\pm\delta}$ multiferroic nanoparticles

Abstract
The effect of particle size on magnetic properties in single-crystalline multiferroic $YMn_2O_{5.07}$ nanoparticles was investigated. A modified Pechini's method was employed to synthesize $YMn_2O_{5.07}$ powders with different particle sizes under an atmosphere of 10 bar O_2. It was found that the multiferroic $YMn_2O_{5.07}$ compound displays a profound size dependence in its magnetic properties when the particles were smaller than 160 nm. With a decrease in particle size, a ferromagnetic-like phase with a broad transition emerges and the transition temperature increases. This ferromagnetic-like phase might be attributed to the surface layer of the nanoparticles and the broad magnetic transition could be caused by the dispersion of particle size and the size dependence of the transition temperature.

Keywords
Curie point, Ferromagnetism, Antiferromagnetism, Nanoparticles, Nanopowders, Annealing, Magnetoelectric effects, Exchange interactions, Magnetic phase transitions, Powders

Comments
The following article appeared in *Journal of Applied Physics* 105 (2009): 033908, and may be found at http://dx.doi.org/10.1063/1.3077263.

Size-dependent magnetic properties of high oxygen content YMn 2 O 5 ± multiferroic nanoparticles

C. Ma, J.-Q. Yan, K. W. Dennis, R. W. McCallum, and X. Tan

Citation: Journal of Applied Physics **105**, 033908 (2009); doi: 10.1063/1.3077263
View online: http://dx.doi.org/10.1063/1.3077263
View Table of Contents: http://scitation.aip.org/content/aip/journal/jap/105/3?ver=pdfcov
Published by the AIP Publishing

Size-dependent magnetic properties of high oxygen content $YMn_2O_{5\pm\delta}$ multiferroic nanoparticles

C. Ma,[1] J.-Q. Yan,[1] K. W. Dennis,[1] R. W. McCallum,[1,2] and X. Tan[1,2,a)]
[1]*Materials and Engineering Physics Program, Ames Laboratory, U.S.-DOE, Ames, Iowa 50011, USA*
[2]*Department of Materials Science and Engineering, Iowa State University, Ames, Iowa 50011, USA*

(Received 13 May 2008; accepted 28 December 2008; published online 10 February 2009)

The effect of particle size on magnetic properties in single-crystalline multiferroic $YMn_2O_{5.07}$ nanoparticles was investigated. A modified Pechini's method was employed to synthesize $YMn_2O_{5.07}$ powders with different particle sizes under an atmosphere of 10 bar O_2. It was found that the multiferroic $YMn_2O_{5.07}$ compound displays a profound size dependence in its magnetic properties when the particles were smaller than 160 nm. With a decrease in particle size, a ferromagnetic-like phase with a broad transition emerges and the transition temperature increases. This ferromagnetic-like phase might be attributed to the surface layer of the nanoparticles and the broad magnetic transition could be caused by the dispersion of particle size and the size dependence of the transition temperature. © *2009 American Institute of Physics*. [DOI: 10.1063/1.3077263]

I. INTRODUCTION

Recently, there has been a worldwide surge in the research on magnetoelectric multiferroic compounds, which exhibit both ferroelectricity and magnetism in the same phase.[1–4] It is the coupling between ferroelectric and magnetic properties that makes multiferroic materials extremely promising for applications in a full line of novel devices, such as multiple state memory elements, electric field controlled ferromagnetic resonance devices, transducers with magnetically modulated piezoelectricity, and devices in the emerging spintronics field.[5]

The RMn_2O_5 family, where R is a rare earth element or yttrium, is one of the very few oxide families which display multiferroism. These RMn_2O_5 compounds crystallize in an orthorhombic structure with the space group *Pbam*. The unit cell contains two crystallographic sites for Mn cations with different oxygen coordinations and oxidation states: Mn^{4+} ions are located at the 4*f* sites and octahedrally coordinated to oxygens, whereas Mn^{3+} ions occupy the 4*h* sites and are bonded by five oxygens, forming a distorted tetragonal pyramid.[6] The crystal structure contains infinite chains of edge-sharing $Mn^{4+}O_6$ octahedra, running along the *c* axis (in *Pbam* notation), and the different chains are interconnected by the $Mn^{3+}O_5$ pyramids and RO_8 scalenohedra.

The RMn_2O_5 compounds are unique because their ferroelectric transition occurs slightly lower in temperature than the antiferromagnetic transition and the ferroelectricity is believed to originate from the magnetic order of the Mn cations.[7–9] In YMn_2O_5, the long range antiferromagnetic order develops at T_N=45 K, while the ferroelectric transition occurs at $T_C \cong 40$ K. Additional magnetic and ferroelectric transitions were observed at ~18 K and the nature of these transitions is still under debate.[10,11] According to neutron diffraction studies, the antiferromagnetic order occurs between the Mn^{3+} and Mn^{4+} spins with magnetic moments in the *ab* plane with a helical structure.[12] The magnetic propagation vector was found to be commensurate with the underlying crystal lattice between around 20 and 45 K, and incommensurate below 20 K.[11,13] It should be pointed out that all the studies so far on YMn_2O_5 or other RMn_2O_5 compounds were performed on either single crystals or polycrystalline ceramics and effects of oxygen stoichiometry and particle size on multiferroic properties have not yet been investigated. Since magnetism and ferroelectricity are both cooperative phenomena and display intrinsic size effect,[14–21] it is of high interest to explore the possible size effect in magnetoelectric multiferroic compounds.[22,23] The present study, which was designed to investigate the magnetic behavior of YMn_2O_5 nanoparticles, revealed both a size effect and a strong dependence on the oxygen partial pressure under which the materials were processed.

II. EXPERIMENTAL PROCEDURE

Nanometric particles of single-phase $YMn_2O_{5\pm\delta}$ compound were prepared by calcining the precursor powder synthesized by a modified Pechini's method. Stoichiometric amount of Y_2O_3 and MnO_2 were dissolved in 15 mol/l nitric acid subsequently. In dissolving MnO_2, 30% H_2O_2 solution was added in drops until dissolution was complete. Then, as a chelating agent, citric acid solution was added in drops to the metal nitrate solution while the solution was magnetically stirred. The molar ratio of citric acid to total metal ions was 1.5:1. The *p*H value of the metal-ion-chelated complex solution was adjusted to 5 by adding aqueous ammonia solution. Then, the clear solution was dried at 150 °C for 12 h to form a gel. The precursor powder was obtained by heating the gel at 600 °C for another 12 h, where all the organics and nitrate ions were removed. The precursor powders were calcined at 800, 900, and 1000 °C, respectively, for 30 h to obtain the final nanoparticles with different sizes. Calcinations were performed in two different oxygen partial pressures, 1 and 10 bar of flowing O_2. For comparison, some of the powder obtained by calcination at 1000 °C was pressed into a pellet. A bulk polycrystalline $YMn_2O_{5\pm\delta}$ ceramic

a)Electronic mail: xtan@iastate.edu.

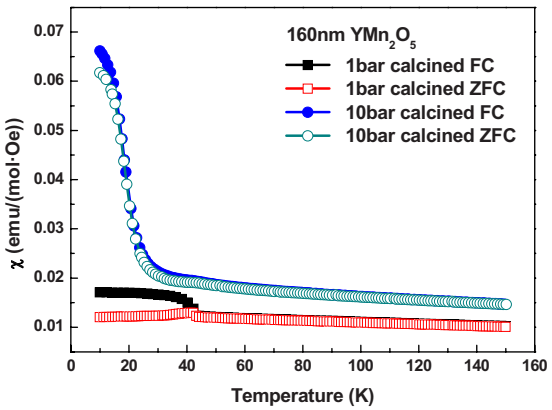

FIG. 1. (Color online) The dc magnetic susceptibility χ vs T curves measured from $YMn_2O_{5\pm\delta}$ particles processed at 1000 °C under 1 and 10 bar oxygen. The particle size is 160 nm under both conditions.

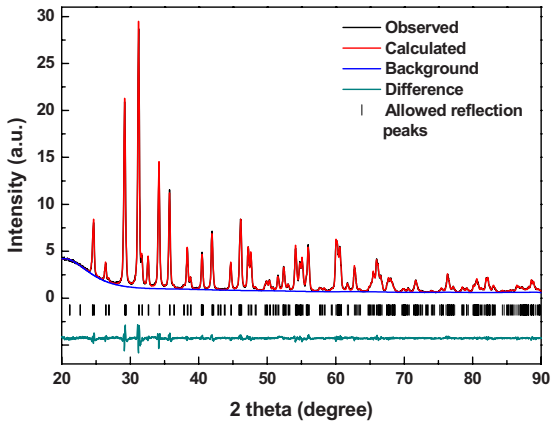

FIG. 2. (Color online) X-ray diffraction pattern of the 160 nm powder refined by Rietveld method.

sample was prepared by sintering this pellet at 1000 °C under 10 bar O_2. Two separate sets of 1000 °C-calcined samples were annealed at 800 and 900 °C, respectively, to adjust the oxygen content to the equilibrium values at those temperatures.

The phase purity of the powders was verified by x-ray diffraction with monochromatic Cu $K\alpha$ radiation. The data were fit using the General Structure Analysis System (GSAS) Rietveld refinement program. Detailed fitting parameters will be reported elsewhere. The particle size was calculated using the Scherrer equation from the fitted peak width. The morphology and crystallinity of the nanoparticles were further examined with an FEI Tecnai F20 transmission electron microscopy (TEM), operated at 200 kV. The oxygen content is determined by the iodometric titration.[24] The magnetic characterization was performed with a Superconducting Quantum Interference Device (SQUID) magnetometer. The hysteresis loops were measured at 5 K. The magnet was conditioned at 150 K and then field cooled to 5 K before the measurement. The dc magnetic susceptibility was measured under a magnetic field of 100 Oe in both field-cooling (FC) and zero-field-cooling (ZFC) conditions. The ac susceptibility was measured under a small oscillating magnetic field of 1 Oe at 1 and 100 Hz in the temperature range of 5–70 K.

III. RESULTS

Distinct differences in magnetic behavior were observed in powder samples calcined at 1000 °C under 1 and 10 bar oxygen atmospheres. As shown in Fig. 1, the powder processed under 1 bar oxygen condition shows a clear slope change at about 45 K, consistent with the published data in previous studies.[25,26] However, this anomaly becomes obscure in the powder processed under 10 bar oxygen condition; the temperature dependence of magnetization is dominated by the anomaly at 20 K. In 100 Oe, the low temperature magnetization of the 10 bar particles is considerably larger than that of the 1 bar particles. In addition, while the 1 bar particles exhibit a large difference between the ZFC and FC curves, the 10 bar particles exhibit practically identical FC and ZFC curves. These differences suggest that, in addition to having an additional anomaly at lower temperature, the net moment of the 10 bar particles is larger, while the domain wall pinning is smaller than that of the 1 bar particles. Iodometric titration of the 1000 °C calcined particles showed that the oxygen content in $YMn_2O_{5\pm\delta}$ formula of the 1 bar material is 4.98 ± 0.01, while that of the 10 bar material is 5.07 ± 0.01. Although we are unable to determine the location of the excess oxygen in the crystal structure at the moment, the results clearly demonstrated the significant role the processing condition plays in determining the magnetic behavior in $YMn_2O_{5\pm\delta}$. Detailed studies on the effect of oxygen stoichiometry on magnetic transitions are under way and will be reported separately. In the present work, we focus on the magnetic properties of oxygen-rich $YMn_2O_{5\pm\delta}$ particles of different sizes processed under 10 bar oxygen atmosphere.

When processed under 10 bar oxygen, the as-calcined $YMn_2O_{5\pm\delta}$ powders display a pure phase which can be indexed based on the *Pbam* space group (Fig. 2). The diffraction peaks are increasingly broadened with the decrease in the calcination temperature, which indicates a decrease in the grain size. According to the calculations using Scherrer equation, the mean sizes of the grains calcined at 800, 900, and 1000 °C are 60, 95, and 160 nm, respectively. The lattice parameters were determined by Rietveld refinement and are listed in Table I. These nanoparticles were further examined with TEM. Representative micrographs are shown in Fig. 3. TEM analysis confirmed the mean size determined by x-ray diffraction and showed that the samples consist of single grain particles. The TEM results also give an estimation of the size distribution. Most of the nanoparticles have an irregular shape. Particles with facets were also observed, as shown in Fig. 3(a). Also seen in Fig. 3 is the thin amorphous

TABLE I. Lattice parameters determined by Rietveld refinement for the $YMn_2O_{5\pm\delta}$ nanoparticles processed under 10 bar oxygen.

Particle size (nm)	a (Å)	b (Å)	c (Å)	V (Å^3)
60	7.261(5)	8.452(5)	5.668(3)	347.8(4)
95	7.273(2)	8.471(2)	5.674(1)	349.6(1)
160	7.274(1)	8.480(1)	5.674(1)	350.0(1)

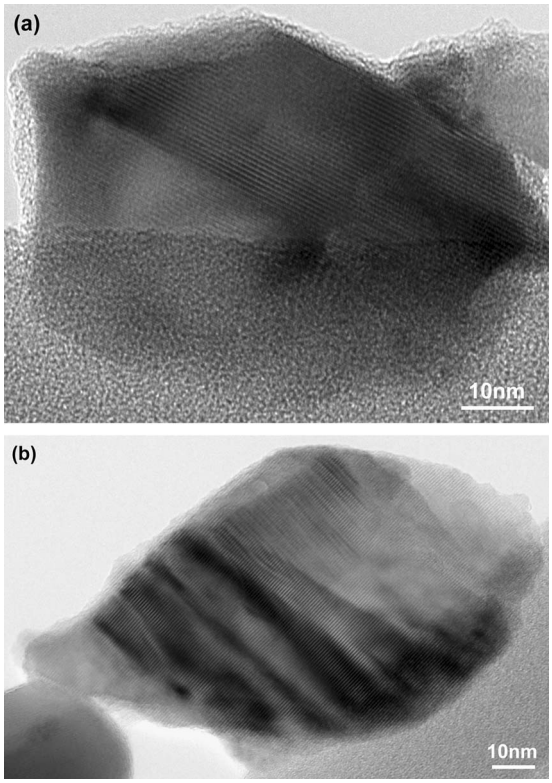

FIG. 3. TEM micrographs of $YMn_2O_{5\pm\delta}$ nanoparticles calcined under 10 bar oxygen at (a) 800 °C and (b) 900 °C.

layer at the surface (~0.01%–0.03% by volume), which slightly thickens as calcination temperature decreases.

The magnetic properties were measured in these single-phase nanoparticles with different particle sizes calcined under 10 bar oxygen. Figure 4 displays the temperature dependence of magnetic susceptibility for the powders with different particle sizes. For bulk and 160 nm samples, the 20 K anomaly is dominant, and the 40 K anomaly is also present but obscure. For powders with particle sizes of 60 and 95 nm, an additional magnetic phase appears with the onset transition temperature at around 70 and 60 K, respectively. Below the onset transition temperature, the susceptibility increases rather gradually over a broad region of around 40 K as temperature decreases. The diffuseness of the transition suggests an inhomogeneous magnetic state. A cusp-like peak at ~15 K, which is not present in the ZFC curve for either bulk or 160 nm sample, appears in the 60 and 95 nm particles and becomes sharper with decreasing particle size. This feature is most likely associated with an increase in coercivity in the smaller particles below the 20 K transition. The temperature where the FC curve deviates away from the ZFC curve increases as the particle size decreases.

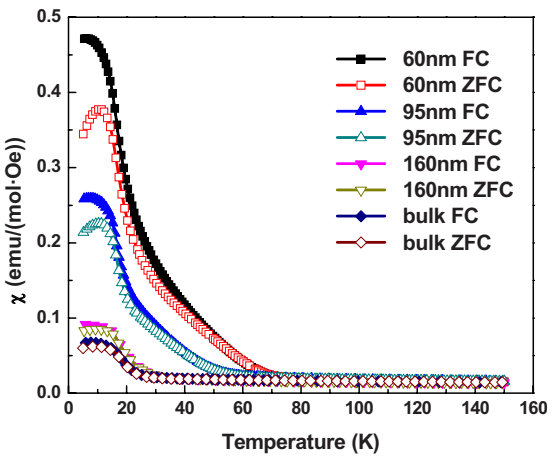

FIG. 4. (Color online) Temperature dependence of the dc susceptibility for powders with different sizes. The measurement was performed at $H = 100$ Oe.

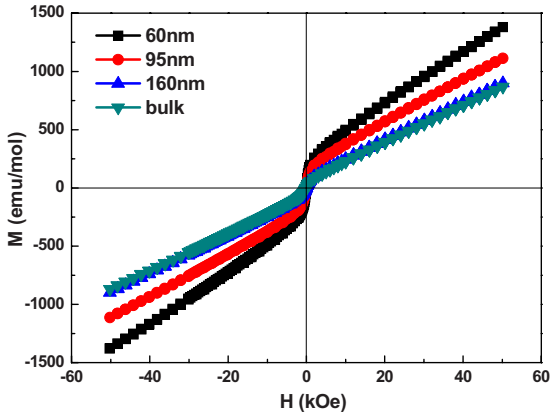

FIG. 5. (Color online) Magnetic hysteresis loops at 5 K for the 60, 95, and 160 nm particles and the bulk ceramic.

The magnetic field-induced magnetization in these powders was assessed at 5 K with a peak field of 5 T. The results which are displayed in Fig. 5 are characteristics of a randomly oriented, nearly compensated ferrimagnet. In this case, the uncompensated moment along the easy axis gives a ferromagnetic-like M versus H curves which saturate at low fields, here about 4 kOe, while M versus H perpendicular to the easy axis has a linear field dependence characteristic of the perpendicular susceptibility of an antiferromagnet. The zero field net moment per Mn atom may be estimated by the intercept of a linear fit of the high field magnetization with the zero field axis. The magnetization in the 160 nm particles is almost the same as that in the sintered bulk ceramic, which yields a moment of 0.01 μ_B/Mn. The induced magnetization at a given magnetic field is strongly size dependent. Both the zero field intercept and the high field slope of the M versus H curves increase with decreasing particle size.

In order to investigate the possibility of superparamagnetism or glass-like transitions in these particles, we performed ac susceptibility measurements under 1 and 100 Hz field. The measurements exhibited no frequency dependence, eliminating relaxation behavior as a cause of the observed effects. Figure 6 shows the temperature dependence of ac susceptibility of particles with different sizes measured in the 1 Hz field. In agreement with the dc measurements, the temperature dependence curves of χ' and χ'' indicate that as the particle size decreases, a broad high temperature transition appears and moves to higher temperature. While there is no indication of the normal 40 K transition in χ', the 20 K transition is clearly visible for all samples, consistent with the dc magnetization. For the 60 nm particles the onset of the

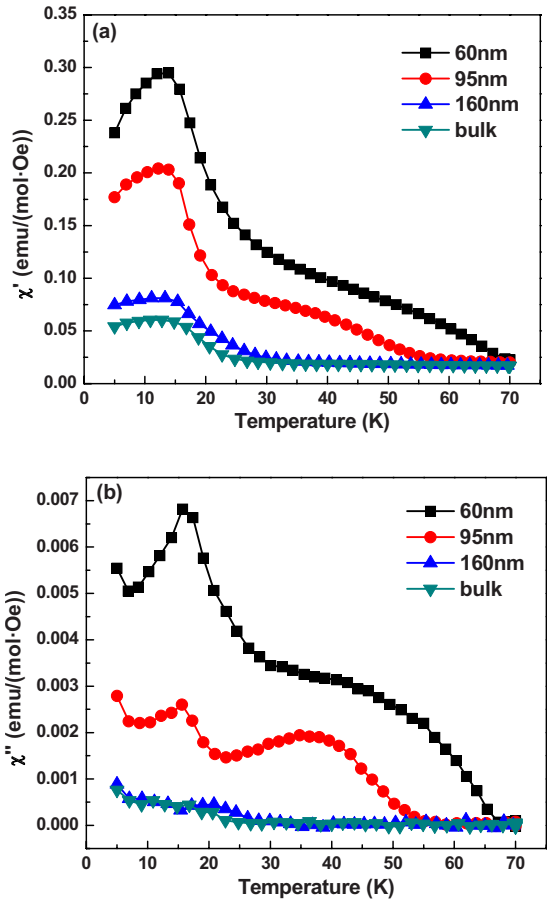

FIG. 6. (Color online) Temperature dependence of the ac susceptibility for powders with different sizes measured at 1 Hz field. (a) The real part χ'. (b) The imaginary part χ''.

high temperature transition is 68 K, significantly higher than any transition previously reported for YMn_2O_5. Thus both the ac and dc measurements are consistent with the normally observed 20 K transition and an obscured 40 K transition in all particle sizes. The smaller particles also exhibit a high temperature transition.

IV. DISCUSSION

The magnetic behavior observed in these oxygen-rich $YMn_2O_{5\pm\delta}$ nanoparticles demonstrates a clear size dependence which may result from either extrinsic and/or intrinsic causes. There are several mechanisms which may induce a size effect in the magnetoelectric multiferroic $YMn_2O_{5\pm\delta}$. For a homogeneous particle which is sufficiently small, one may expect to see a quantum effect due to the finite size of the system. However, the fact that the smallest mean particle size in our study is 60 nm, together with the apparent two-phase nature of the transition in these particles, suggests that this is highly unlikely to be the origin of the observed effect. It is well known that ferroelectric oxides such as $BaTiO_3$ and $PbTiO_3$ display a critical size below which lattice distortion as well as spontaneous polarization vanishes.[14–17] Such ferroelectric size effect was observed before to induce changes in magnetic properties in multiferroic $BiFeO_3$.[22,23] However, this mechanism is not likely to be applicable to our material since RMn_2O_5 compounds are improper ferroelectrics and it is believed that the spontaneous polarization is induced by the magnetic ordering of Mn cations.[7–9]

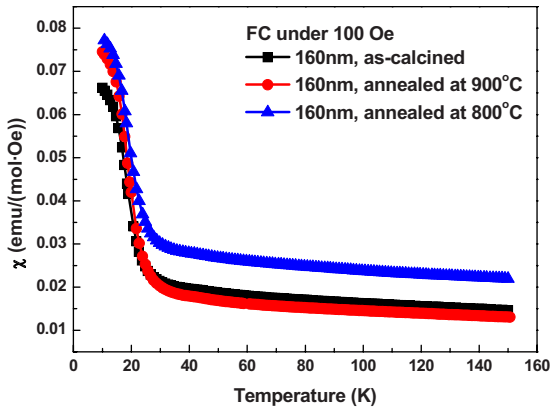

FIG. 7. (Color online) Temperature dependence of the dc susceptibility for the as-calcined 160 nm powder and the 160 nm powder annealed at 800 and 900 °C.

As we have already noted, there is a strong effect of the oxygen partial pressure during calcinations on the magnetic properties of $YMn_2O_{5\pm\delta}$. Thus a possible explanation is that the oxygen content of the particles is a function of the calcination temperature. Unfortunately, it is not possible to vary the particle size without varying the calcination temperature. However, it is possible to vary the oxygen level of large particles by annealing them at the calcination temperature of the smaller particles. Therefore, we annealed two separate batches of 1000 °C as-calcined $YMn_2O_{5\pm\delta}$ powder (with a mean particle size of 160 nm) at 800 °C (at which the 60 nm particles were produced) and 900 °C (at which the 95 nm particles were produced) under 10 bar O_2. The annealing was for 30 h at both temperatures. This is the same amount of time used when the precursor powder was calcined at these two temperatures. During the annealing, the 160 nm particles are not expected to grow in size since the annealing temperature is lower than the initial calcination temperature, which was also confirmed by the study of (112) Bragg peak using Scherrer equation. In this way, the annealed powder is assumed to have the same equilibrium oxygen content as the original 800 and 900 °C as-calcined powders but the same particle size (160 nm) as the 1000 °C as-calcined powder. If any change in the magnetic response is observed in the annealed powders from the as-calcined 160 nm powder, such change will be directly from the oxygen defect effect. As shown in Fig. 7, the 900 °C annealed powders showed no change. The transition temperature of the 800 °C annealed powders was unchanged, but there was an increase in the high temperature susceptibility. This increase was linear in field so it does not represent a ferromagnetic impurity. In neither case was the 70 K transition observed. More investigation to understand the lack of anomaly at 70 K for an annealed sample is in process and this will be addressed later.

If the phenomena observed in the smaller particles result from a core-shell type microstructure, we should be able to estimate the minimum thickness of the shell from the magnetization measurements. From the sintered pellet, the core magnetization is estimated at 0.01 μ_B/Mn, assuming a fer-

romagnetic shell with a moment of the order of 2 μ_B/Mn and a shell thickness of the order of 0.1 nm. Given this minimum thickness, the possibility of an intrinsic effect due to uncompensated surface spins in a crystallographically ordered surface should be considered. An antiferromagnetic material can be considered as a combination of one sublattice with spins along one direction and another with spins along the opposite direction. If no spin canting is considered, the spins of these two sublattices compensate each other so that the net magnetization inside the material should be equal to zero. However, on the surface of the material, this compensation is interrupted. Néel[18] attributed the large magnetic moment and emergence of ferromagnetic-like behavior in small antiferromagnetic particles to this incomplete spin compensation on the surface. With the decrease in the particle size, the specific surface area increases, so the uncompensated surface spins become more significant to the whole system, and the magnetic response to the applied field would become stronger and more ferromagnetic-like with the decrease in the particle size. However, this intrinsic effect cannot be responsible for the phenomena observed here since uncompensated surface spins in this model can only be observed below the Néel temperature. The magnetic ordering in the 60 and 95 nm particles occurs around 70 K, well above the highest Néel temperature of YMn_2O_5 ever reported in literature (45 K).[10]

Given the low volume fraction of ferromagnetic phase required to account for the observed magnetization, the possibility that there is an impurity phase not associated with the main phase nanoparticles must be addressed. The required volume fraction is well below that which can be detected by x-ray diffraction and the sampling in TEM is far too limited to rule out second phase particles. However, close examination of Fig. 5, presented in Fig. 8(a), indicates the presence of an exchange bias in each hysteresis loop. With the decrease in the particle size, the exchange bias decreases and the coercivity increases, as listed in Table II and replotted in Fig. 8(a). In Fig. 8(b), hysteresis data for the 60 nm particles are presented for three different cooling conditions, ZFC which shows minimal bias, and FC with cooling fields of 8 and −8 kOe where the bias reverses consistent with exchange bias. The presence of the exchange bias requires that the ferromagnetic and the antiferromagnetic components be in intimate contact within the same particle. The size dependence of the coercivity is easily explained in terms of micromagnetic models of the coercivity of single-grain single domain particles[27] which predict that H_c for noninteracting particles is inversely proportional to the square of the diameter, $H_c=(a/d^2)-b$. Using the data summarized in Table II, the correlation coefficient between H_c and $1/d^2$ is calculated as 0.9997, confirming the expected result. The size dependence of the exchange bias is complicated by the fact that there are two contributions to the hysteresis, the small uncompensated moment of the core and the reversal of the moment of the more ferromagnetic shell and will be discussed below. However, the fact that the exchange bias is present in the low temperature hysteresis loops indicates that the ferromagnetic and antiferromagnetic phases exist in the same particle.

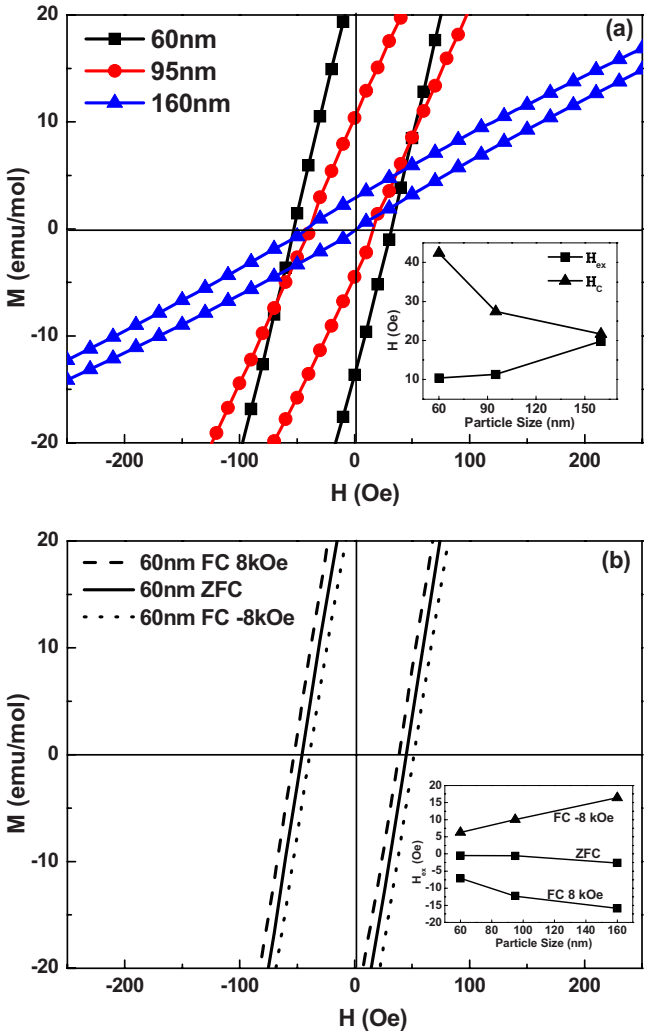

FIG. 8. (Color online) (a) Close view of the M vs H hysteresis loops in $YMn_2O_{5\pm\delta}$ nanoparticles shown in Fig. 5. Inset: the exchange bias H_{ex} and coercivity H_c of the nanoparticles as a function of the particle size. (b) Close view of the M vs H hysteresis loops of 60 nm $YMn_2O_{5\pm\delta}$ nanoparticles measured at 5 K under ZFC, 8 kOe FC, and −8 kOe FC conditions, respectively. Inset: the exchange bias H_{ex} of $YMn_2O_{5\pm\delta}$ nanoparticles with different particle sizes under ZFC, 8 kOe FC, and −8 kOe FC conditions.

More insight into the nature of the core-shell structure may be gained by studying the M versus H curves at low temperature. Formally the data in Fig. 5 can be represented as

$$M(H) = M_{\mathrm{FM}}(H) + \chi_{\mathrm{AF}}H, \tag{1}$$

where χ_{AF} is the high field slope ($H>4$ kOe) describing the linear portion of the curve.

χ_{AF} is the integral of the projection of the perpendicular susceptibility of the antiferromagnet over our random grain distribution. $M(H)$ is characterized by a saturation value M_s

TABLE II. Magnetic parameters derived from hysteresis loops at 5 K.

d (nm)	$1/d^2$ (nm^{-2})	M_s (μ_B/Mn)	χ_{AF} (emu/Oe mol)	H_{ex} (Oe)	H_c (Oe)
60	2.78×10^{-4}	0.030	0.021	10.4	42.4
95	1.11×10^{-4}	0.021	0.017	11.3	27.4
160	3.91×10^{-5}	0.010	0.016	19.8	21.7

given by the intercept of the linear fit to the high field susceptibility with the zero field axis. The intercept is composed of two contributions. First, there is a contribution which is due to the integral of the projection of the parallel susceptibility of the antiferromagnet over our random grain distribution from the not perfectly compensated spins. This accounts for the step at low field observed in the 160 nm particles and the sintered sample shown in Fig. 5. The second contribution is from the ferromagnetic shell which saturates at low field. Thus the ferromagnetic contribution may be estimated from the size dependence of the intercept assuming that the core antiferromagnetic structure is independent of size.

The calculated values of χ_{AF} and M_s are listed in Table II. When the particle size decreases, both χ_{AF} and M_s increase. The increase in M_s reflects the growing volume fraction of the ferromagnetic shell. There are two possible explanations for the observed increase in χ_{AF}: either the anisotropy of the particles is a function of size or the amorphous phase fraction is largely antiferromagnetic with an enhanced perpendicular susceptibility in the smaller particles. The size dependence of the H_{ex} is directly related to the increase in M_s with decreasing particle size. Generally for a system possessing an intimate contact between ferromagnetic and antiferromagnetic phases, H_{ex} is inversely proportional to M_s.[28] As a result, a larger exchange bias is observed for the 160 nm particles. The decrease in thickness of the ferromagnetic layer also contributes to the higher exchange bias.

In the above discussion, the amorphous surface layer observed in the TEM study of the smaller particles has been ignored. Based on the volume fraction estimated above, it would appear that the fraction of amorphous material is actually too large to account for the observed ferromagnetic component. However that estimate was based on assuming that the shell was ferromagnetic with a full Mn moment. A more plausible mechanism to account for the ferromagnetic component is that only short to intermediate range order exists in the apparently amorphous shell. Such short range spin order could result in a magnetic structure similar to that of the crystalline core but with a higher transition temperature and a larger uncompensated moment due to changes in the longer range magnetic interactions. The resulting moment would be considerably below that of a long range ferromagnetic order. The existence of disorder in the longer range interactions within the amorphous phase would also explain the broadness of the high temperature magnetic transition. From this analysis, it appears that the size dependence of the M versus T curves is an extrinsic effect due to the presence of an amorphous shell on the particles.

V. CONCLUSIONS

The magnetic properties of multiferroic $YMn_2O_{5\pm\delta}$ nanoparticles display a profound size dependence when the particle size is less than 160 nm. A ferromagnetic-like component emerges and its susceptibility is enhanced as the particle size decreases. The coercivity increases while the exchange bias decreases with decreasing particle size. The onset temperature of the ferromagnetic transition increases as the particle size decreases: with a value of ~60 K for the 95 nm particles and 70 K for the 60 nm particles. For both particle sizes below the onset transition temperature the magnetic susceptibility increases almost linearly with decreasing temperature over a range of about 40 K and does not saturate prior to the ordering of the antiferromagnetic phase at 20 K. The observed size effect could be well explained by a model describing the nanoparticle as an antiferromagnetic core with an extrinsic amorphous or poorly crystallized shell displaying a higher transition temperature and a substantially larger specific moment. The broad transition of the ferromagnetic-like surface layer is consistent with such a shell where inhomogeneous short to medium range order results in a broad distribution of transition temperatures.

ACKNOWLEDGMENTS

Work at the Ames Laboratory was supported by the Department of Energy, Basic Energy Sciences under Contract No. DE-AC02-07CH11358.

[1] T. Kimura, T. Goto, H. Shintani, K. Ishizaka, T. Arima, and Y. Tokura, Nature (London) **426**, 55 (2003).
[2] R. Ramesh, A. Inam, W. K. Chan, B. Wilkens, K. Myers, K. Remshing, D. L. Hart, and J. M. Tarascon, Science **252**, 944 (1991).
[3] J. Wang, J. B. Neaton, H. Zheng, V. Nagarajan, S. B. Ogale, B. Liu, D. Viehland, V. Vaithyanathan, D. G. Schlom, U. V. Waghmare, N. A. Spaldin, K. M. Rabe, M. Wuttig, and R. Ramesh, Science **299**, 1719 (2003).
[4] M. Fiebig, J. Phys. D **38**, R123 (2005).
[5] I. B. Shim, J. H. Yeom, K. R. Choi, C. S. Kim, H. J. Shin, and S. Y. An, J. Appl. Phys. **95**, 7070 (2004).
[6] J. A. Alonso, M. T. Casais, M. J. Martínez-Lope, J. L. Martínez, and M. T. Fernández-Díaz, J. Phys.: Condens. Matter **9**, 8515 (1997).
[7] L. C. Chapon, P. G. Radaelli, G. R. Blake, S. Park, and S.-W. Cheong, Phys. Rev. Lett. **96**, 097601 (2006).
[8] M. V. Mostovoy, Phys. Rev. Lett. **96**, 067601 (2006).
[9] Y. Noda, H. Kimura, Y. Kamada, and T. Osawa, Physica B **385–386**, 119 (2006).
[10] K. Kohn, Ferroelectrics **162**, 1 (1995).
[11] I. Kagomiya, S. Nakamura, S. Matsumoto, M. Tanaka, and K. Kohn, J. Phys. Soc. Jpn. **74**, 450 (2005).
[12] G. Buisson, Phys. Status Solidi A **16**, 533 (1973).
[13] J. J. Betouras, G. Giovannetti, and J. van den Brink, Phys. Rev. Lett. **98**, 257602 (2007).
[14] K. Uchino, E. Sadanaga, and T. Hirose, J. Am. Ceram. Soc. **72**, 1555 (1989).
[15] T. Yamamoto, K. Urabe, and H. Banno, Jpn. J. Appl. Phys., Part 1 **32**, 4272 (1993).
[16] W. L. Zhong, B. Jiang, P. L. Zhang, J. M. Ma, H. M. Cheng, Z. H. Yang, and L. X. Li, J. Phys.: Condens. Matter **5**, 2619 (1993).
[17] S. Chattopadhyay, P. Ayyub, V. R. Palkar, and M. Multani, Phys. Rev. B **52**, 13177 (1995).
[18] L. Néel, Compt. Rend. **252**, 4075 (1961).
[19] J. Nogués, J. Sort, V. Langlais, V. Skumryev, S. Suriñach, J. S. Muñoz, and M. D. Baró, Phys. Rep. **422**, 65 (2005).
[20] R. H. Kodama, S. A. Makhlouf, and A. E. Berkowitz, Phys. Rev. Lett. **79**, 1393 (1997).
[21] E. Galstyan, B. Lorenz, K. S. Martirosyan, F. Yen, Y. Y. Sun, M. M. Gospodinov, and C. W. Chu, J. Phys.: Condens. Matter **20**, 325241 (2008).
[22] T. J. Park, G. C. Papaefthymiou, A. J. Viescas, A. R. Moodenbaugh, and S. S. Wong, Nano Lett. **7**, 766 (2007).
[23] S. M. Selbach, T. Tybell, M. Einarsrud, and T. Grande, Chem. Mater. **19**, 6478 (2007).
[24] F. Licci, G. Turilli, and P. Ferro, J. Magn. Magn. Mater. **164**, L268 (1996).
[25] A. M. Kadomtseva, Y. F. Popov, G. P. Vorobev, K. I. Kamilov, P. N. Makhov, M. M. Tehranchi, and A. Phirouznia, Physica B **329–333**, 856 (2003).
[26] T. C. Han and J.G. Grace, J. Appl. Phys. **99**, 08J508 (2006).
[27] R. C. O'Handley, *Modern Magnetic Materials, Principles, and Applications* (Wiley, New York, 1999).
[28] M. S. Seehra and A. Punnoose, Solid State Commun. **128**, 299 (2003).